RSC Advances

ROYAL SOCIETY OF CHEMISTRY

www.rsc.org/advances

RSC Advances

ARTICLE

Refractometric and colorimetric index sensing by plasmon-coupled hybrid AAO nanotemplate

Received 00th January 20xx,
Accepted 00th January 20xx

DOI: 10.1039/x0xx00000x

www.rsc.org/

Kyuyoung Bae,[a] Jungmin Lee,[a] Gumin Kang,[a] Do-sik Yoo,[b] Chang-Won Lee*[c] and Kyoungsik Kim*[a]

Facile optical sensors capable of measuring small change of analytes' refractive indices have been highlighted as the demand of environmental and Internet-of-Things (IoT) applications increased. In this work, we demonstrate large-area refractive index sensor feasible refractometric and colorimetric sensing with plasmon-coupled hybrid nanotemplate of anodic aluminum oxide (AAO). The nanotemplate enhances figure-of-merit and sensitivity owing to coupled mode of Fabry-Perot microcavity and metallic nanosurfaces. The increased mode confinement and interaction between AAO pores and analytes show highly modulated reflection spectra, which enables refractive index sensitivity up to 348 nm/RIU and figure-of-merit value up to 27.7. Also, vivid color change induced from infiltrated analytes allows colorimetric sensing performance up to RIU/ΔE ~ 0.006 according to CIELab 1931 analysis. The key features of our device are simultaneous applications to superb dual (refractometric and colorimetric) sensing schemes by plasmon-coupled hybrid AAO nanotemplate.

Introduction

Late advancements in nanotechnology have prompted new applications for optical sensors that can measure a broad range of chemical or biomolecular analytes in environmental and Internet-of-Things (IoT) applications.[1–10] In order to apply optical sensors to IoT applications, it is required to have small form factor with minimal power consumption. In addition, acquired data need to be transmitted and analyzed in a simple way without external batteries. Therefore it is very feasible to use smartphones or digital cameras for optical sensing since they are already well-distributed, easy to use and have computational powers enough to analyze data.

The optical sensors detect the electromagnetic spectrum shift arising from the refractive index change when analyte target approaches to active region.[11] Generally, two approaches have been available for index sensing: refractometric and colorimetric. Refractometric sensing analyses shifted transmission or reflection spectrum owing to electromagnetic interaction between the active region and target analytes. Therefore, a spectroscopic setup is necessary for capturing and analysing spectrum. On the other hand, colorimetric sensing uses no external device and just uses recognized color change. For refractometric index sensing, methods such as polarimetric measurement,[12] resonance spectrum shift of surface plasmon of gold with molecular labeling,[13,14] and light waveguide based on anodic aluminum oxide (AAO)[15–17] have been successfully demonstrated. For colorimetric index sensing, color changes of silver nanovolcano array,[18] 1D nanotemplate based on mixed metal oxide (MMO) -TiO2,[19] coupled silicon nanowire arrays[20] and gold nanopatch array[21] have been measured and analysed.

Among various optical sensors, surface plasmon resonances (SPR) sensor has been intensively studied owing to its ability to enhance the local electromagnetic field at the nanoscale.[22,23] SPR sensors are very sensitive to the change of the dielectric permittivity within the active region, where the interaction between the plasmonic nanostructure and the analyte takes place. The local electromagnetic mode can be detected by far-field spectroscopy through radiative damping process.[24] One of the most significant problems of the SPR-based sensor is broad plasmonic resonance due to large absorption loss of metals. The broad linewidth limits important sensing characteristics - the figure-of-merit (FOM), which is defined as the refractive index sensitivity divided by spectral linewidth.[23,25–27] Another problem of SPR-based sensor is small spatial sensing depth of active region, which is only constrained to a few nanometers around the plasmonic nanostructure[26,28,29]. Therefore, a sophisticated micro-spectroscopic setup is required to collect far-field efficiently and measure the spectrum.

To overcome these problems, several methods have been proposed to enhance the sensitivity, FOM, and detection scheme of SPR-based sensors. First, strong coupling of broad SPR resonance to a system with narrow plasmonic resonance by Fano effect[30–32] or electromagnetically induced transparency[33,34] have been proposed. The strongly coupled system can be introduced by the propagating mode in a periodic grating[35] or coupling between individual metallic rods.[24,31,35] The coupled mode shows altered plasmonic resonance

[a] School of Mechanical Engineering, Yonsei University, 50 Yonsei-ro, Seodaemun-gu, Seoul 120-749, Korea. E-mail: kks@yonsei.ac.kr
[b] School of Electronic and Electrical Engineering, Hongik University, 94 Wausan-Ro, Mapo-Gu, Seoul 121-791, Republic of Korea.
[c] Samsung Advanced Institute of Technology, Suwon, Korea. E-mail: cwlee42@gmail.com
* Corresponding authors

spectra to more asymmetric and narrower shapes, which provides higher FOM and sensitivity for refractive index sensing. Second method is to use plasmonic waveguide structure.[36,37] Change of the plasmonic mode due to filled analyte in a hollow metallic cavity leads to enhanced sensitivity and FOM. Third method is to use coupling SPR resonance to an optical microcavity to decrease the resonance linewidth.[38–41] The linewidth of such a hybrid resonance can be reduced by the modified cavity Q factor determined by radiative damping of the coupled system.

However, all these methods require lithographic fabrication process and sophisticated spectroscopic setup in order to obtain high refractive index sensitivity and FOM. In this paper, we demonstrate a facile method to fabricate large area and low-cost template for coupling SPR and optical Fabry-Perot microcavity. AAO template with deposited metal nanosurface is used not only to couple electromagnetic modes, but also to simplify analyte infiltration scheme. The plasmon-coupled modes enhance the electromagnetic field and the interaction with the analyte at the AAO-air interface to make Fabry-Perot mode have large Q-factors. AAO template is employed as the fabrication method is simple in spite of its nanoscale structure compared to electron beam lithography, which is commonly used for nanofabrication. Excellent chemical and mechanical stability of aluminum oxide, also, led AAO template to be applied.[42] Moreover, structure parameters of AAO such as thickness and pore diameter of AAO template are readily controllable with anodization and pore widening time.[43,44] The coupled mode can greatly enhance sensitivity and FOM for efficient sensing of analyte's refractive index. In addition, we observe vivid color change allowing simple colorimetric sensing either by naked eyes or cheap digital camera. It has been shown that the hybrid plasmon-coupled AAO system excellently combines the advantages of Fabry–Perot microcavities with those of plasmonic nanostructures, providing exceptional features such as large spatial sensing depth and perceptually recognizable colorimetric sensing.

We first design and fabricate refractive index sensor based on hybrid plasmon-coupled AAO templates for analyte targets with refractive indices from 1.4 ~ 1.7. In order to obtain large spectral shift and color change, we study the effect of the gold nanosurfaces and AAO microcavity with thickness less than 500 nm. Using finite-difference time-domain (FDTD) simulations, we provide a detailed explanation of the underlying physics of the hybrid plasmon-coupled AAO structure and the expected reflectance spectra depending on the thickness of the templates and refractive indices of analytes. Then, we analysed the images of the AAO template taken by a digital camera on the basis of CIELab 1931 color space to study perceptual colorimetric sensor performance. We find the computed Euclidean distances between the tristimulus points in the color space strongly depend on the AAO thicknesses. We find AAO with 250 nm thickness shows the largest color sensitivity at normal viewing angle. For further enhancement of the refractometric sensitivity and FOM, we increased AAO thickness up to 5 μm. We find the sensitivity and FOM follow same trend in the energy scale rather than in wavelength scale. The effect of annealing of deposited gold nanosurface with respect to colorimetric and refractometric sensing performances have been investigated as well. The gold layer turns into gold nanoparticles when annealed in high temperature, and the change of localized surface plasmon resonances and Fabry-Perot interference affects the performance of the hybrid plasmon-coupled AAO structure.

Experimental

Fabrication of plasmon-coupled AAO templates

The conventional two step anodization process was performed from high purity aluminum foil (99.999%) with a thickness of 0.5 mm to get well-ordered hexagonal AAO array.[45] The first anodization was carried out under a constant voltage of 40 V in 0.3M oxalic acid solution at 10℃ so that we could get a hexagonal array with interpore distances of ~ 100 nm. After the first anodization, the AAO layer was removed in a mixture of 1.8wt% chromic acid and 6wt% phosphoric acid for 4 h at 80℃. After the AAO layer was completely etched, the second anodization was carried out under the same condition at 1 to 5 min, and 1 h for thin and thick thicknesses of aluminum oxide layer of AAO template, respectively. Afterwards, the AAO template was chemically etched in an aqueous solution of 5wt% phosphoric acid solution for 24 min at 30℃ to widen the pore diameter to 70 nm. Lastly, the gold nanosurface was deposited by sputtering on the surface of AAO template.

Characterization

For refractometric index sensing, the reflection spectra were measured using a fiber-coupled UV-VIS-NIR spectrometer (Ocean optics USB2000+). The emitted white light from a Tungsten Halogen light source were coupled into a reflection fiber probe (R400-7-VIS-NIR). The measurement was performed in a wavelength range from 400 nm to 1000 nm and a reference silver mirror was used as a calibration reflection measurement. As test analytes, Cargille refractive index fluids were used to control refractive indices ranging from 1.35 to 1.7. After each measurement, the plasmon-coupled AAO template was rinsed carefully with acetone and distilled water without changing position of the template.

Results and Discussion

Design and Fabrication of hybrid plasmon-coupled AAO templates

A schematic of the hybrid optical sensor, composed of Fabry-Perot microcavity for narrow resonance and metal nanosurfaces for broad SPR resonance, is illustrated in Fig. 1(a). Under the illumination from top of the AAO template, some of the light is reflected back from the top of the AAO structure with phase change ϕ_1. Some of the light is transmitted into the AAO microcavity and partly reflected back from the bottom of the AAO structure. After one round-trip inside the cavity, the light is partly transmitted back out of the top of the AAO microcavity with phase change ϕ_2. The phase difference of the light totally reflected back from the AAO microcavity determines Fabry-Perot interference conditions; $\phi_2 - \phi_1$ =

$(2n+1)\pi$ or $(2n)\pi$ with integer n for destructive and constructive interference, respectively. The phase difference for the reflected light corresponds to 4π nL/λ, where n, L and λ are refractive index of the cavity, cavity length, and the wavelength of light, respectively. Therefore, for a given Fabry-Perot cavity, the cavity length and the modal wavelength are proportional to each other. Also, for a given spectral bandwidth, thicker cavity length leads to more modes in shorter wavelength.

While the Fabry-Perot cavity mode is determined by the thickness of the AAO template, the strength of the coupling with metal nanosurfaces depends on whether the metal nanosurfaces are located at the node or at the anti-node of the Fabry-Perot mode.[40] In a typical Fabry-Perot cavity, their field localization is very poor so that the support of SPR is limited. However, our porous Fabry-Perot cavity structure increases the interaction length between the cavity and the infiltrated analyte, and the phase shifts ϕ_1 and ϕ_2 can be greatly affected by the SPR of top metal nanosurfaces. In thicker AAO structure, the phase accumulation is more important to keep several round-trips of the light inside the microcavity.

Scanning electron microscope (SEM) images show that AAO template has well-ordered hexagonal array with average pore size of 70 nm and the average lattice between the pores of 100 nm, as shown in Fig. 1(b). The sputtered gold forms rough surface on the surface of AAO surface with average thickness of 10 nm. Side-view SEM image shows that most of the gold is deposited on the surface of AAO template (Fig. 1(c)).

Using a commercial finite-difference time-domain (FDTD) package (Lumerical Solutions Inc.), we simulate reflectance spectra to find the resonant mode of the hybrid plasmonic AAO structure with respect to the cavity length. First, we assume the pores in AAO are empty without analyte. We also assume the sputtered gold nanosurfaces as a uniformly deposited gold layer with 10 nm thickness. Fig. 2 (a) shows the normalized reflectance as a function of wavelength and of AAO thickness. The reflectance spectrum modulations owing to Fabry-Perot modes can be clearly observed as a linear color region in the color contour map as functions of the AAO thickness and the wavelength. For a fixed AAO thickness, reflectance spectrum shows modulated Fabry-Perot resonance conditions with increasing wavelength. Likewise, the modulation depth increases with increased AAO thickness. At 638 nm, as shown as a horizontal while dotted line, sharp reflectance valley is observed. The reflectance valley corresponds to a destructive interference of Fabry-Perot mode owing to the gold nanosurface's plasmon resonance.

In order to find the effect of the sputtered gold nanosurfaces on the Fabry-Perot mode, we simulate reflectance spectra of 300 nm-thick AAO microcavities for the cases with and without gold layers, as shown in Fig. 2(b). The red solid line and dotted line denote the simulated reflectance spectra AAO with and without thin gold layer, respectively. Without gold nanosurfaces, Fabry-Perot mode of the pristine AAO template does not show any sharp modulation depth. The resultant FOM derived from the reflection peak (or valley) without gold nanosurfaces is low. On the other hand, the simulation shows a sharp negative peak near the valley at 638 nm owing to the surface plasmon resonance (SPR) of gold. In addition, the reduced reflection at the valley further enhances FOM.

Refractometric index sensing by hybrid plasmon-coupled AAO templates

We measured reflection spectrum to find out the sharp negative peak at 638 nm. Unfortunately, this negative peak could not be experimentally observed, as seen from the black solid line in Fig 2(b). According to our speculation, the negative peak is smeared out

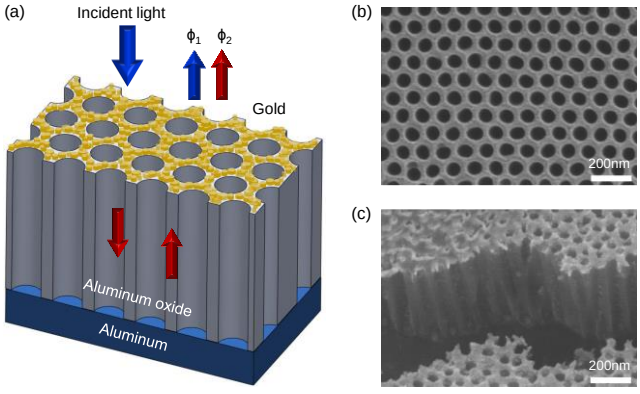

Fig. 1 (a) Schematic illustration of plasmonic AAO nanotemplate. The AAO template is grown on the aluminum substrate and the gold is sputtered on the AAO template. The thickness of AAO template can be tuned by anodization time. The arrows show incident and reflected light paths through the structure. (b) The scanning electron microscope (SEM) image for top AAO nanostructure shows well-ordered hexagonal array with average pore size of 70 nm and the average lattice between the pores of 100 nm. The gold layer of ~ 10 nm was sputtered on the surface of AAO template. The sputtered gold forms a nanosurface with small empty holes and rough surface. (c) Side-view SEM image of the AAO nanostructure shows that most of the gold is deposited on the surface of AAO template and few gold particles are attached on the side walls.

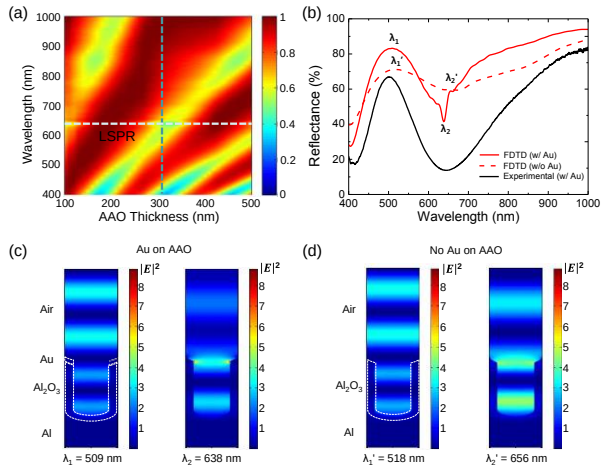

Fig. 2 (a) Simulated normalized reflectance is shown as a color contour as a function of the thickness of AAO template and illumination wavelength for cavity-coupled plasmonic structure described in Fig. 1. (b) Simulated (red) reflectance spectra by finite-difference time-domain method and measured (black) spectra are drawn with (solid) and without (dash) gold layer. The AAO template thickness is 300 nm. Sputtered gold layer on the AAO template enhances modulation depth of Fabry-Perot mode. Simulated electric field intensity distributions are shown with gold layer (c) for the peak (λ_1 = 509 nm) and valley (λ_2 = 638 nm), and without gold layer (d) for the peak (λ_1' = 518 nm) and valley (λ_2' = 656 nm), respectively. The plasmonic absorption is shown in (c) at the wavelength of the valley of the reflectance spectrum (λ_2) near the gold layer.

due to imperfect hexagonal AAO lattice structure and nonuniform layer thickness. Without the sharp negative peak, though, the reduced reflection valley near 630 nm by gold sputtering leads to enhanced FOM of the peak at 509 nm. We also note the reflectance at 509 nm increases 10 % with AAO with gold nanosurfaces. The increased modulation depth of the Fabry-Perot mode serves better for refractive index sensing.

Mode profiles at reflectance peaks and valleys are shown in Fig. 2(c) and (d) for the AAO with gold layer (c) for the peak (λ_1 = 509 nm) and valley (λ_2 = 638 nm), and without gold layer (d) for the peak (λ_1' = 518 nm) and valley (λ_2' = 656 nm), respectively. Regardless of the gold nanosurfaces, standing wave pattern can be observed both inside and outside the AAO microcavity. Mode profiles at λ_1 and λ_1' show constructive interference allowing large reflection from the AAO microcavity. Whereas mode profiles at λ_2 and λ_2' show destructive interference and highly confined mode within the AAO microcavity. Even though the field difference outside the cavity at λ_1 and λ_1' is not significant (10% change in the Fig. 2(b)), the field difference outside the cavity at λ_2 and λ_2' is very large. Therefore, the reflectance spectrum modulation depth for the case with gold nanosurfaces is larger than the case without gold nanosurfaces. The enhanced modulation depth in reflectance spectrum leads to higher FOM for analyte index sensing.

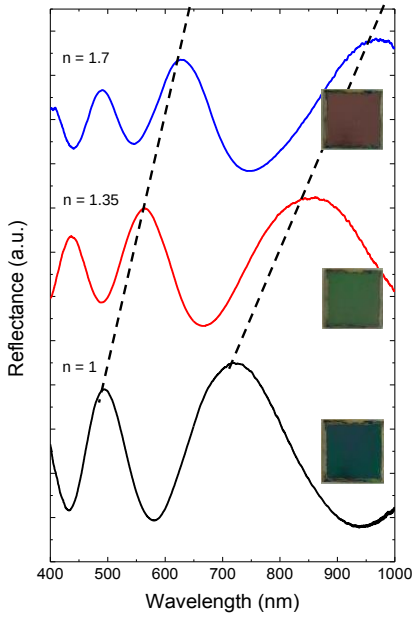

Fig. 3 Refractometric index sensing using plasmonic AAO nanostructure. Measured reflectance spectra of the plasmonic AAO nanostructure by changing surrounding medium with different refractive index (n = 1 - 1.7) when AAO template thickness is 500 nm. The peaks are shifted to longer wavelength with constant rate as the refractive index of surrounding medium increases. With this thickness 500 nm of AAO template, sensitivity of ~ 324 nm/RIU is obtained. The color images of the AAO templates with analytes are shown in right.

In order to enhance reflectance spectrum modulation depth, we increase AAO hybrid cavity thickness to 500 nm for refractometric sensing scheme. Cargille refractive index fluids, which are stable and wettable to the AAO surface, are used as test analytes to control refractive index values 1.35 and 1.7.[20] As analytes with higher refractive index infiltrate into the AAO template, the reflection spectrum moves to longer wavelength pushing up the resonance condition of the hybrid plasmonic AAO structure changes, as shown in Fig. 3. Within the detector range in the visible, the peaks at longest wavelength show large shift after analytes infiltration. As a result, the peak shift is linearly proportional to the refractive index of the analytes with maximum sensitivity of ~ 324 nm/RIU.

Colorimetric index sensing by hybrid plasmon-coupled AAO templates

With the AAO template with infiltrated analyte, we observed significant color changes, suggesting our AAO template can be used as a colorimetric sensor. The color of the prepared AAO microcavity is affected by all the interference peaks. Since the color depends on the cavity structure and material's dielectric permittivity, refractive index change can be perceptually recognized by color gamut analysis.[46] The color can be changed with respect to the viewing angle as well as the analyte refractive index.

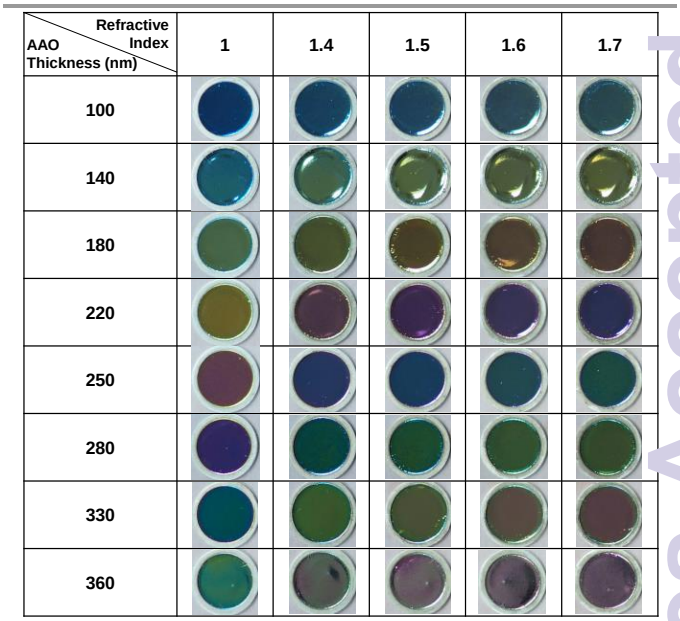

Fig. 4 Optical images of the AAO templates as a function of the tested refractive index immersion liquids and thickness of AAO template from 100 nm to 360 nm. All images are taken by a digital camera at normal viewing angle under identical illumination condition. The color change with 100 nm thick AAO microcavity is not noticeable, whereas those with 180 ~ 330 nm thickness show vivid color changes.

In order to figure out the best thickness for colorimetric sensor, eight AAO templates with thicknesses from 100 nm to 360 nm have been examined regarding four different analytes with refractive indices from n = 1.40 to n=1.70, as shown in Fig. 4. The 100 nm-thick AAO sensor shows little color change, whereas AAO sensors with thickness from 180 nm to 330 nm show large color changes with the infiltrated analyte targets.

Based on the optical images taken by a digital camera, we evaluate the colorimetric sensing performance of our hybrid AAO microcavity by mapping the image data to CIELab 1976 chromaticity diagram, as shown in Fig. 5. One of the advantages of the CIELab color representation is device-independence so that

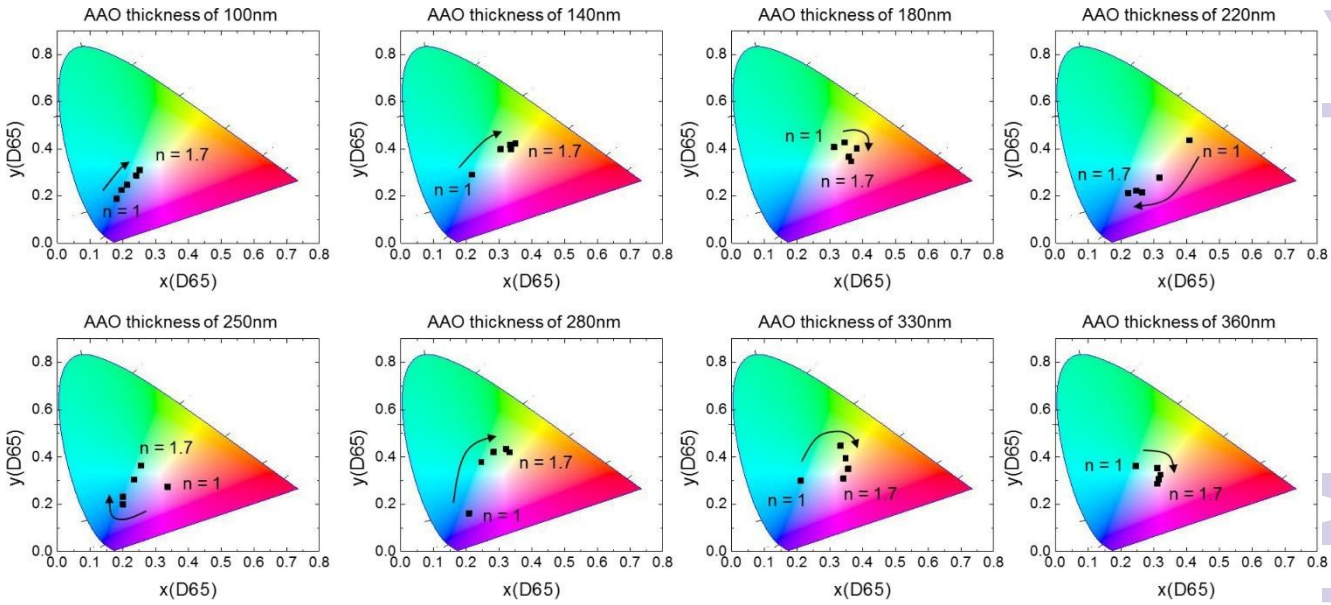

Fig. 5 CIELab points of the plasmonic AAO sensor are shown as a function of refractive indices of analytes and various AAO template thicknesses ranging from 100 nm to 360 nm. With increasing refractive index of the analytes, the measured (L*, a*, b*) color points rotate clockwise.

comparing with other photographed images are possible.[47] All colors in CIELab coordinate can be represented by tristimulus values; [46] lightness L^* and chromaticities a^* and b^*. Lightness L^* component closely matches human perception of lightness. Quantitative color difference between the two colors, denoted by ΔE meaning Euclidean distance between the two color points, is given by the following formula:

$$\Delta E = \sqrt{\Delta L^{*2} + \Delta a^{*2} + \Delta b^{*2}}\,, \qquad (1)$$

where ΔL^*, Δa^*, Δb^* are the differences between two arbitrary points in lightness L^* and chromaticities a^* and b^* axes. ΔE can be used as a standardized indicator for perceived color difference by an observer.46 The approximate minimal threshold of perceptual color change corresponds to $\Delta E \sim 1.46$ It should be noted that auxiliary factors such as surrounding background radiation, illumination conditions, and observer perception may affect ΔE.

Table 1.

AAO Thickness	ΔE n = 1 - 1.4	n = 1.4 - 1.5	n = 1.5 - 1.6	n = 1.6 - 1.7	RIU/ΔE
100nm	8.77	5.10	**8.83**	5.74	0.011
140nm	25.20	**6.78**	5.39	5.10	0.015
180mn	10.77	**12.25**	7.55	7.81	0.008
220nm	42.06	**13.00**	5.92	4.90	0.008
250nm	24.92	10.00	**15.62**	11.22	0.006
280nm	**49.68**	8.94	8.25	6.16	0.008
330nm	31.59	**14.04**	11.70	10.25	0.007
360nm	20.49	**10.63**	8.60	6.56	0.009

Calculated Eucledean distances between two refractive indices with respect to the AAO microcavity thickness. The largest distance is for each AAO thickness is shown in boldface. The calculated minimum refractive index unit for the perceptual color change is shown in the right column.

As refractive indices of test analytes increase, the calculated tristimulus values move clockwise, as shown in Fig. 5. Therefore, appropriate sensing device should be chosen for specific analyte's refractive index. Table 1 shows the calculated Euclidean distances for the refractive index change of the analytes. Because the tristimulus values do not monotonically increase with increasing refractive index of analytes, the actual path in the CIELab space along continuous index change is longer than the Euclidean distance between two points apart. Therefore, the calculated RIU/ΔE is interpreted as the lower limit of the colorimetric sensing performance of our AAO microcavity. The AAO microcavities with 180 ~ 330 nm thicknesses show no larger than RIU/ΔE = 0.01. The best perceptual refractive index change is RIU/ΔE ~ 0.006 when $\Delta n = 0.1$.

Enhanced FOM with increasing AAO thickness

As long as good Fabry-Perot mode is maintained, the thicker AAO microcavity provides more number of modal peaks. This in turn leads to narrower peak or valleys with increased modulation depth. Therefore, increasing anodizing time may pave the way to increase such a modulation depth and FOM. FOM is defined by $\mathrm{FOM} = (d\lambda/dn)/\Delta\lambda$ or $(dE_p/dn)/\Delta E_p$ depending on the domain unit.[39] Here, $\Delta\lambda$ and ΔE_p are FWHMs of a peak in reflectance spectrum in the unit of wavelength (nm) and of photon energy (eV) respectively.

One of the major issues of increasing cavity length is that the intensity of total reflected light in the AAO microcavity decreases owing to the light absorption and inelastic light scattering inside the AAO pores. For this purpose, good reflectivity at top and bottom of the AAO template are necessary. We kept increasing the AAO thickness up to 5 μm as long as gold nanosurface is coated on the top surface. As a result, total reflection from the AAO template generates sharper interference peaks, as shown in Fig. 6(a). Without sputtered gold nanosurfaces, we find the modulation depth of the

AAO microcavity becomes poor, as shown in Fig. 6(b). Therefore, the peak shifts are not clearly recognized after analyte infiltration due to the broad reflectance peaks. The sputtered gold nanosurface on top of the AAO microcavity plays important role of increasing reflections and keeping phase shifts. In addition, stable Fabry-Perot mode and the resultant large FOM is achieved even with the imperfections of the AAO microcavity.

In order to compare sensitivity and FOM in the same spectral domain, we plot the extracted sensitivities (red dots) and FOMs (blue dots) as a function of wavelength and as a function of photon energy, as shown in Fig 6(c) and Fig. 6(d), respectively. In the wavelength domain, sensitivity up to 348 nm/RIU and FOM up to 27.7 can be obtained. One of the interesting features of the FOM in the wavelength domain is that FOM behaves oppositely to the sensitivity, as shown in Fig. 6(c). This implies that the domain of the refractometric refractive index sensing should be more carefully chosen. In the energy domain as shown in Fig. 6(d), sensitivities and FOMs follow same trend. This means that FOM serves better characteristics for refractive index sensing in the high energy, i.e. in short wavelength region. Even though FOM serves as a kind of normalized unitless sensitivity, only the FOM defined in the energy domain provides same physical interpretation as sensitivity.

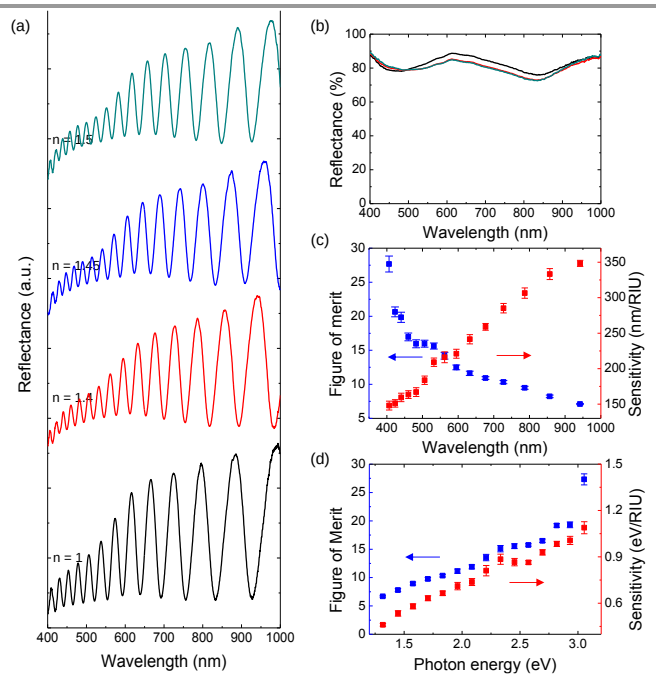

Fig. 6 (a) Measured reflectance spectra of the plasmonic AAO nanostructure by changing surrounding medium with different refractive index (n = 1 – 1.5) when AAO template thickness is 5 μm. (b) Reflectance spectra of the AAO structure without gold layer. There are no changes as the refractive index of surrounding medium increases. (c) Sensitivity and FOM of plasmonic AAO nanostructure at the different peak center of AAO as a function of wavelength (nm). High sensitivities are obtained at longer wavelengths and high figure of merits are attained at shorter wavelengths. Although the sensitivity is getting lower as the peak wavelength decreases, the figure of merit increases due to the smaller FWHM. Maximum sensitivity of 348 nm/RIU is obtained. (d) Sensitivity and FOM of the same plasmonic AAO nanostructure as a function of photon energy (eV). They have same trend in the energy domain.

Annealing Effect of hybrid plasmon-coupled AAO templates

We have attempted to enhance the color purity by annealing gold nanosurface on AAO template 500℃ for 2 hours. The annealing leads to deformation of the sputtered gold nanosurface and to color change owing to the resultant phase change ϕ_1 of the top interface, as shown in Fig. 7(a). SEM images taken before (b) and after (c) the annealing process show that rough gold nanosurface transforms to nanoparticles. As the gold nanosurface transforms to nanoparticles, plasmonic effect is enhanced while gold-covered area is reduced. Consequently, the hybrid Fabry-Perot mode is changed. However, we find the annealing does not produce significant colorimetric performance enhancement.

Instead, we observe that annealing can enhance refractometric sensing performance in a special condition. Fig. 8 shows reflectance spectra change with enhanced sensitivity for 280 nm-thick AAO with n = 1.4 analyte. The sensitivity from the shortest wavelength peak increases from 217 nm/RIU to 282 nm/RIU owing to the annealing effect. However, AAOs with other thicknesses ranging from 150 nm to 500 nm do not produce enhanced refractometric sensing performances. Further investigations are required for optimized annealing conditions for index sensing.

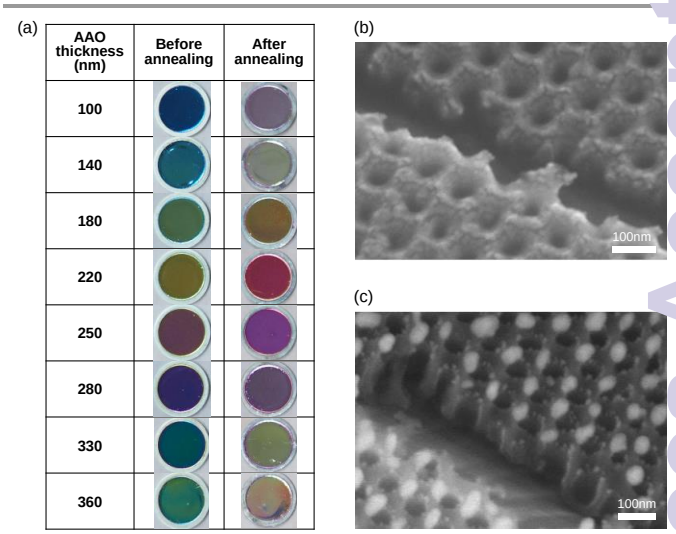

Fig. 7 (a) Optical images of the AAO templates as a function of the tested refractive index immersion liquids and before/after annealing process. Annealing process was performed at 500° for 2 hours. All images were taken by a digital camera at normal viewing angle under identical illumination condition. The all colors change for all thicknesses of AAO because agglomerated gold particles developed by annealing process enhance localized surface plasmon resonance and reduce Fabry-Perot interference. (b) SEM image of the plasmonic AAO nanostructure before annealing process. (c) SEM image of the AAO nanostructure after annealing process. Gold clusters agglomerate together to form nanoparticles with diameter of 20 – 50 nm and smaller particles near the pores of AAO template.

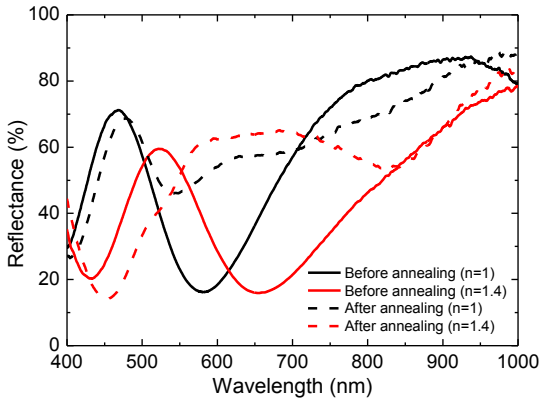

Fig. 8 Refractometric index sensing using plasmonic AAO nanostructure of bare samples (solid lines) and annealed samples (dashed lines). Reflectance spectra of the plasmonic AAO nanostructure were measured in the air and infiltrating surrounding medium with refractive index of 1.4 when AAO template thickness is 280 nm. The peaks are shifted to longer wavelength as the surrounding medium infiltrated and the annealed plasmonic AAO nanostructure shows more red-shift. The sensitivity from the shortest wavelength peak increases from 217 nm/RIU to 282 nm/RIU owing to the annealing effect.

Conclusions

In summary, we have introduced a facile approach to achieve a high sensitive refractive index sensor using AAO nanostructures, which combines the advantages of Fabry–Perot microcavities with local surface plasmonic resonance induced by gold nanosurfaces. The reflectance spectrum under ambient illumination is linearly shifted due to the refractive index change of the infiltrated analyte with respect to the air. The gold nanosurfaces play significant roles to form hybrid resonances arising from the constructive and destructive interference. High sensitivity and FOM were attained with 5μm AAO template for refractometric sensing. The FOM of the spectra was examined to extract the most sensitive peak shift from the reflectance data; a sensitivity of 1.14 eV/RIU, and a FOM of 27.7 at an optical wavelength of around 406 nm. We observed that sensitivity and FOM behave proportional in the photon energy domain, but inversely in the wavelength domain with respect to the peak of reflectance spectrum. The obtained highest sensitivity reaches 348 nm/RIU in wavelength domain. Clear color changes by refractive index variation were achieved with AAO template thickness of under 500nm for colorimetric sensing scheme. With the advantage of the proposed large scale feature with sensitive color change by simple infiltration of the analyte, we examined visually recognizable sensing characteristics by analyzing CIELab mapping of the images taken by a conventional camera. Small refractive index changes down to ~ 0.006 RIU can be obtained with respect to perceptual color change recognition over a whole visible range.

Our sensor provides not only refractometric sensing scheme with high sensitivity, but also quite decent colorimetric sensing performance by naked eyes or cheap cameras for quick preliminary inspections. It is also possible to use as biosensors if receptors are pre-prepared either on top of or inside the AAO template for selectivity function. The reflective phase shift of Fabry-Perot mode can be changed by binding with analyte biomolecules. Since the mode change is proportional to the filling of the analyte inside the AAO pores, liquid type analyte seems unavoidable. If gaseous biomolecules in the air can be sufficiently condensed and the resultant index of the gas is changed, gaseous analytes might be applicable. Our approach is a promising candidate for low-cost and highly sensitive detection of multiple analytes in a simple and rapid format, and would allow applications to other chemical systems, sensing for food industry, and IoT devices.

Acknowledgements

This research was supported by Basic Science Research Program and the Pioneer Research Center Program through the National Research Foundation of Korea (NRF) funded by the Ministry of Science, ICT and Future Planning (NRF-2015R1A2A2A11001112, NRF-2013M3C1A3065045), the Low Observable Technology Research Center program of the Defense Acquisition Program Administration and Agency for Defense Development and an Asian Office of Aerospace R&D grant, FA2386-15-1-4024 (15IOA024). The authors gratefully thank to Yeon Hong Kim for careful feedback and discussions.

References

1 J. Homola, S. S. Yee and G. Gauglitz, Sensors Actuators B Chem., 1999, 54, 3–15.
2 A. J. Haes and R. P. Van Duyne, J. Am. Chem. Soc., 2002, 124, 10596–10604.
3 J. Homola, Anal. Bioanal. Chem., 2003, 377, 528–39.
4 S. M. Borisov and O. S. Wolfbeis, Chem. Rev., 2008, 108, 423–61.
5 S. Zeng, K.-T. Yong, I. Roy, X.-Q. Dinh, X. Yu and F. Luan, Plasmonics, 2011, 6, 491–506.
6 X. Guo, J. Biophotonics, 2012, 5, 483–501.
7 I. Singh, Int. Journals Nanosensors, 2015, 1, 1–7.
8 C. L. Baird and D. G. Myszka, J. Mol. Recognit., 2001, 14, 261–8.
9 W.-P. Chen, F.-H. Shih, P.-J. Tseng, C.-H. Shao and C.-C. Chiang, Sensors Journal, IEEE, 2015, 15, 734–741.
10 J. Lee, K. Bae, G. Kang, M. Choi, S. Baek, D. Yoo, C.-W. Lee and K. Kim, RSC Adv., 2015, 5, 71770–71777.
11 M. Bahramipanah, M. S. Abrishamian, S. A. Mirtaheri and J.-M. Liu, Sensors Actuators B Chem., 2014, 194, 311–318.
12 J. Álvarez, C. Serrano, D. Hill and J. Martínez-Pastor, Opt. Lett., 2013, 38, 1058–1060.
13 S.-H. Yeom, M.-E. Han, B.-H. Kang, K.-J. Kim, H. Yuan, N.-S. Eum and S.-W. Kang, Sensors Actuators B Chem., 2013, 177, 376–383.
14 H. M. Hiep, H. Yoshikawa and E. Tamiya, Anal. Chem., 2010, 82, 1221–1227.
15 A. Yamaguchi, K. Hotta and N. Teramae, Anal. Chem., 2009, 81, 105–111.
16 K. Hotta, A. Yamaguchi and N. Teramae, Anal. Chem., 2010, 82, 6066–6073.
17 K. Hotta, A. Yamaguchi and N. Teramae, ACS Nano, 2012, 6, 1541–1547.

18 B. Ai, Y. Yu, H. Möhwald and G. Zhang, Adv. Opt. Mater., 2013, 1, 724–731.
19 Y. Dou, J. Han, T. Wang, M. Wei, D. G. Evans and X. Duan, J. Mater. Chem., 2012, 22, 14001–14007.
20 M. Khorasaninejad, N. Abedzadeh, J. Walia, S. Patchett and S. S. Saini, Nano Lett., 2012, 12, 4228–4234.
21 M. K. and S. M. R.-Z. and H. A. and N. A. and S. S.-N. and S. S. Saini, Nanotechnology, 2013, 24, 355501.
22 J. Homola, Chem. Rev., 2008, 108, 462–493.
23 M.-C. Estevez, M. A. Otte, B. Sepulveda and L. M. Lechuga, Anal. Chim. Acta, 2014, 806, 55–73.
24 R. Ameling, L. Langguth, M. Hentschel, M. Mesch, P. V. Braun and H. Giessen, Appl. Phys. Lett., 2010, 97, 0–3.
25 Y. Shen, J. Zhou, T. Liu, Y. Tao, R. Jiang, M. Liu, G. Xiao, J. Zhu, Z.-K. Zhou, X. Wang, C. Jin and J. Wang, Nat. Commun., 2013, 4, 2381.
26 J. N. Anker, W. P. Hall, O. Lyandres, N. C. Shah, J. Zhao and R. P. Van Duyne, Nat Mater, 2008, 7, 442–453.
27 L. Tong, H. Wei, S. Zhang and H. Xu, Sensors (Basel)., 2014, 14, 7959–73.
28 K. M. Mayer and J. H. Hafner, Chem. Rev., 2011, 111, 3828–3857.
29 A. G. Brolo, Nat Phot., 2012, 6, 709–713.
30 J. B. Lassiter, H. Sobhani, J. A. Fan, J. Kundu, F. Capasso, P. Nordlander and N. J. Halas, Nano Lett., 2010, 10, 3184–3189.
31 a. Christ, Y. Ekinci, H. H. Solak, N. a. Gippius, S. G. Tikhodeev and O. J. F. Martin, Phys. Rev. B - Condens. Matter Mater. Phys., 2007, 76, 3–6.
32 B. Gallinet and O. J. F. Martin, ACS Nano, 2011, 5, 8999–9008.
33 N. Liu, L. Langguth, T. Weiss, J. Kastel, M. Fleischhauer, T. Pfau and H. Giessen, Nat Mater, 2009, 8, 758–762.
34 S. Zhang, D. Genov, Y. Wang, M. Liu and X. Zhang, Phys. Rev. Lett., 2008, 101, 1–4.
35 A. Farhang, T. Siegfried, Y. Ekinci, H. Sigg and O. J. F. Martin, J. Nanophotonics, 2014, 8, 83897.
36 Z.-D. Zhang, H.-Y. Wang and Z.-Y. Zhang, Plasmonics, 2012, 8, 797–801.
37 Xiao-Ping Jin, Xu-Guang Huang, Jin Tao, Xian-Shi Lin and Qin Zhang, IEEE Trans. Nanotechnol., 2010, 9, 134–137.
38 D. Chanda, K. Shigeta, T. Truong, E. Lui, A. Mihi, M. Schulmerich, P. V Braun, R. Bhargava and J. A. Rogers, Nat Commun, 2011, 2, 479.
39 M. A. Schmidt, D. Y. Lei, L. Wondraczek, V. Nazabal and S. A. Maier, Nat Commun, 2012, 3, 1108.
40 D. Choi, C. K. Shin, D. Yoon, D. S. Chung, Y. W. Jin and L. P. Lee, Nano Lett., 2014, 14, 3374–3381.
41 M. Bahramipanah, S. Dutta-Gupta, B. Abasahl and O. J. F. Martin, ACS Nano, 2015, 9, 7621–7633.
42 G. Kang, J. Yoo, J. Ahn and K. Kim, Nano Today, 2015, 10, 22–47.
43 H. M. and M. Satoh, Jpn. J. Appl. Phys., 1996, 35, L126.
44 G. Kang, K. Bae, M. Nam, D.-H. Ko, K. Kim and W. J. Padilla, Energy Environ. Sci., 2015, 8, 2650–2656.
45 H. Masuda and K. Fukuda, Sci. , 1995, 268 , 1466–1468.
46 J. Schanda, Colorimetery: Understanding the CIE System, John Wiley & Sons, 2007.
47 M. M. Hawkeye and M. J. Brett, Adv. Funct. Mater., 2011, 21, 3652–3658.

• A table of contents entry: graphic, maximum size 8 cm x 4 cm and one sentence of text, maximum 20 words, highlighting the novelty of the work

A highly versatile and low-cost large-area refractive index sensor capable of refractometric and colorimetric sensing were developed by a plasmon-coupled hybrid nanotemplate of anodic aluminum oxide with deposited gold nanosurface.

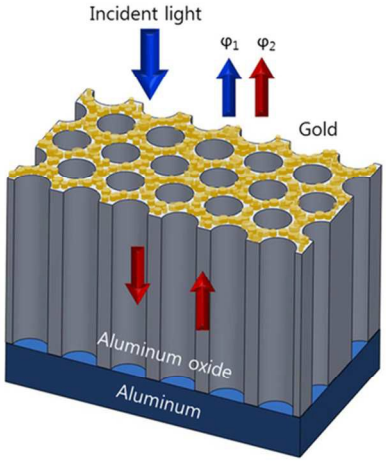

AAO Thickness \ Refractive Index	1	1.4	1.7
220nm			
250nm			
280nm			
330nm			

40x20mm (600 x 600 DPI)